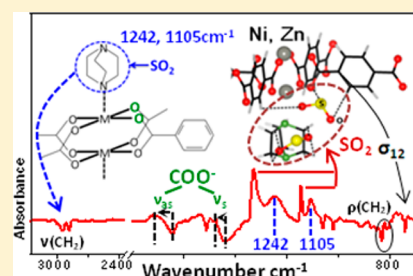


Mechanism of Preferential Adsorption of SO₂ into Two Microporous Paddle Wheel Frameworks M(bdc)(ted)_{0.5}Kui Tan,[†] Pieremanuele Canepa,[‡] Qihan Gong,[§] Jian Liu,^{||} Daniel H. Johnson,[‡] Allison Dyevoich,[§] Praveen K. Thallapally,^{||} Timo Thonhauser,[‡] Jing Li,[§] and Yves J. Chabal^{*,†}[†]Department of Materials Science & Engineering, University of Texas at Dallas, Richardson, Texas 75080, United States of America[‡]Department of Physics, Wake Forest University, Winston-Salem, North Carolina 27109, United States of America[§]Department of Chemistry and Chemical Biology, Rutgers University, Piscataway, New Jersey 08854, United States of America^{||}Energy and Environment Directorate, Pacific Northwest National Laboratory, Richland, Washington 99352, United States of America

S Supporting Information

ABSTRACT: The selective adsorption of a corrosive gas, SO₂, into two microporous pillared paddle-wheel frameworks M(bdc)(ted)_{0.5} [M = Ni, Zn; bdc = 1,4-benzenedicarboxylate; ted = triethylenediamine] is studied by volumetric adsorption measurements and a combination of *in situ* infrared spectroscopy and *ab initio* density functional theory (DFT) calculations. The uptake of SO₂ in M(bdc)(ted)_{0.5} at room temperature is quite significant, 9.97 mol/kg at 1.13 bar. The major adsorbed SO₂ molecules contributing to the isotherm measurements are characterized by stretching bands at 1326 and 1144 cm⁻¹. Theoretical calculations including van der Waals interactions (based on vdW-DF) suggest that two adsorption configurations are possible for these SO₂ molecules. One geometry involves an SO₂ molecule bonded through its sulfur atom to the oxygen atom of the paddle-wheel building unit and its two oxygen atoms to the C–H groups of the organic linkers by formation of hydrogen bonds. Such a configuration results in a distortion of the benzene rings, which is consistent with the experimentally observed shift of the ring deformation mode. In the other geometry, SO₂ establishes hydrogen bonding with –CH₂ group of the ted linker through its two oxygen atoms simultaneously. The vdW-DF-simulated frequency shifts of the SO₂ stretching bands in these two configurations are similar and in good agreement with spectroscopically measured values of physisorbed SO₂. In addition, the IR spectra reveal the presence of another minor species, characterized by stretching modes at 1242 and 1105 cm⁻¹ and causing significant perturbations of MOFs vibrational modes (CH_x and carboxylate groups). This species is more strongly bound, requiring a higher temperature (~150 °C) to remove it than for the main physisorbed species. The adsorption configurations of SO₂ into M(bdc)(ted)_{0.5} derived by infrared spectroscopy and vdW-DF calculations provide the initial understanding to develop microporous metal organic frameworks materials based on paddlewheel secondary-building units for SO₂ removal in industrial processes.

KEYWORDS: metal organic frameworks, paddlewheel, sulfur dioxide, adsorption isotherm, *in situ* infrared spectroscopy, DFT calculations



1. INTRODUCTION

Metal organic frameworks (MOFs) are a new class of solid porous materials that are attracting great interest as a potential material for gas storage and separation because of their extraordinary surface areas and fine-tunable surface properties.^{1–3} Until now, MOFs have been widely investigated for the storage and separation of H₂, CH₄, CO₂, and hydrocarbons.^{3–9} Studies to explore the use for MOFs for harmful gases (e.g., SO₂, H₂S, NO) adsorption and removal are relatively sparse compared to studies on their use for hydrogen storage and carbon capture.^{10–13} In the past decades, adsorption of SO₂ into porous materials such as porous carbon, zeolites has been proposed and investigated by different techniques in order to develop industrial desulfurization process.^{14–19} Recently, Zn-MOF-74 has been found to improve the SO₂ adsorption by a factor of 3 compared to activated carbons and be the best

performing MOF among six prototypical MOFs.²⁰ Very recent breakthrough measurements showed that Mg-MOF-74 provides a better adsorption of SO₂ gas than other MOF-74 series (with Zn, Ni, Co).²¹ Indeed, MOF-74 [M₂(dhtp), dhtp = 2,5-dihydroxyterephthalate] compounds have hexagonal one-dimensional pores containing a high density of coordinatively unsaturated open metal sites that can potentially interact with guest molecules (see Figure S1 in Supporting Information). Usually the generation of MOF structures with exposed metal sites such as MOF-74 compounds is regarded as an effective means to enhance their affinity toward gases.^{3,4} More recently, there has been an effort to develop structures that have

Received: April 18, 2013

Revised: October 22, 2013

Published: October 25, 2013



cooperative multiple interactions with guest molecules that are believed to improve the adsorption capacity.^{22–24} For example, Schröder and co-workers reported a new nonamine-containing MOF complex called NOTT-300, which selectively adsorbs SO₂ to a level of 8.1 mmol/g at ambient temperature and 1.0 bar. The highlight of this finding is that OH group and C–H groups of benzene cooperatively interact with guest SO₂ molecules.²⁴

To develop the understanding of MOF-based materials for SO₂ removal, we examined SO₂ adsorption in a prototypical metal organic framework M(bdc)(ted)_{0.5} [M = Ni, Zn; H₂bdc = 1,4-benzenedicarboxylic; ted = triethylenediamine] and characterized the guest–host interaction by *in situ* infrared spectroscopy and isotherm measurements. Our results show that high SO₂ capacity uptake can be achieved even when using coordinatively saturated MOFs M(bdc)(ted)_{0.5}, at levels up to 9.97 mmol/g at room temperature and 1.13 bar. Combining infrared spectroscopy and first principles calculations, the adsorption mechanism of SO₂ within this class of MOFs is explored. Multipoint interactions between SO₂ molecules and MOFs are found as possible binding sites within the frameworks: SO₂ interacting (i) with the O site of the paddlewheel building units through its sulfur atom and (ii) with the C–H_x groups on the organic linkers through its oxygen atoms.

2. EXPERIMENTAL SECTION

Synthesis. A mixture of nickel(II) chloride hexahydrate (0.107 g, 0.45 mmol), H₂bdc (0.060 g, 0.36 mmol), ted (0.033 g, 0.29 mmol), and 15 mL of DMF were transferred to Teflon-lined autoclave and heated at 120 °C for 2 days. Green crystalline powder of Ni(bdc)(ted)_{0.5} was isolated by filtering and washed three times with 10 mL of DMF. (Yield: 83.8% based on the metal) Then, the sample was heated at 120 °C again under a flow of dry N₂ for one day to remove the guest DMF molecules.

A mixture of zinc(II) nitrate hexahydrate (0.245 g, 0.82 mmol), H₂bdc (0.136 g, 0.97 mmol), ted (0.073 g, 0.65 mmol), and 15 mL of DMF were transferred to Teflon-lined autoclave and heated at 120 °C for 2 days. Cubic colorless crystals of Zn(bdc)(ted)_{0.5} were isolated by filtering and washed three times with 10 mL of DMF. (Yield: 84.5% based on the metal) Then the sample was heated at 120 °C again under a flow of dry N₂ for 1 day to remove the guest DMF molecules.

Infrared Spectroscopy. A powder of M(bdc)(ted)_{0.5} (~2 mg) was pressed onto a KBr pellet (~1 cm diameter, 1–2 mm thick) and placed into a high pressure high temperature cell purchased from Specac (product number P/N 5850c) at the focal point of the sample compartment of the infrared spectrometer (Nicolet 6700, Thermo Scientific) equipped with a liquid N₂-cooled MCT-B detector. The cell was connected to a vacuum line for evacuation. SO₂ gas was introduced into the pressure cell and all spectra were recorded in transmission between 400 and 4000 cm⁻¹ (4 cm⁻¹ spectral resolution). The pressure was determined by calibrating the SO₂ gas IR absorption at low pressures (3 Torr) with a convection gauge (KJL 285801, KurtJLeskerCo) and then using the integrated IR absorption to determine the higher pressures since there is no dependence of the internal mode dipole moment on pressure.

Adsorption Isotherm. Measurements of SO₂ uptake were performed using a volumetric system specially constructed for low-pressure experiments (see Supporting Information Figure S12). It comprises two chambers, A and B, whose volumes have been determined using helium. Chamber B is loaded with the sample and chamber A is a gas reservoir. A known amount of powder sample was placed in chamber B (volume = 4.134 cm³) with a layer of glass wool on top to prevent sudden suction of the powder sample. The sample was activated at 150 °C for 12 h with dynamic vacuum before each measurement. The activated sample weight was measured after experiment and was used to calculate the SO₂ adsorption results.

The activated sample weight for Ni(bdc)(ted)_{0.5}, Zn(bdc)(ted)_{0.5}, and Mg-MOF-74 are 75.5 mg, 94.2 mg, and 95.6 mg, respectively. The activated sample was sealed in chamber B under vacuum. SO₂ (the total impurity of SO₂ gas is less than 0.1% and the water concentration is less than 0.01%) was introduced into chamber A, and then, the valve connecting chamber A and B was opened to let the gas adsorption reach equilibrium. This step was repeated as necessary to obtain the adsorption data points. As for the desorption part, a similar but reverse procedure was adopted. The chamber A was evacuated (1 × 10⁻⁴ Torr), and then, the valve connecting chamber A and B was opened to let the gas desorption reach equilibrium. This step was also repeated as necessary to obtain all desorption data points. The criterion for equilibrium was that the change in pressure was less than 0.1% within 15 min. A longer equilibrium time (1 h) was used but no significant difference was observed for the pressure readings. The SO₂ quantity change was determined by the pressure change in chamber A and B. The recorded pressures were used to calculate the adsorbed amount based on basic mass balance equations. An ideal gas law was adopted and the volume of the sample was estimated to be 0.15 cm³ and need to be subtracted from the volume of chamber A in the calculations. The nonideality of SO₂ was accounted by using the compressibility factor of SO₂, which is 0.99 under our experiment conditions. The activation procedure described above was repeated before proceeding to the next cycle of SO₂ adsorption and desorption measurements. Based on our experimental observations, the Ni(bdc)(ted)_{0.5} can maintain its SO₂ capacity after at least five full cycles of adsorption and desorption.

DFT Calculations. The theoretical results presented in this manuscript were obtained using the van der Waals exchange and correlation functional vdW-DF^{25,26} as implemented in the Vienna Ab Initio Simulation Package, VASP.^{27–30} This functional has already been successfully applied to a number of similar studies, investigating small molecule adsorption in MOFs.^{31–35} vdW-DF is able to accurately describe the weak van der Waals forces originating from nonlocal interactions. We simulated the loading and the coadsorption of SO₂ in M(bdc)(ted)_{0.5}, with M = Ni, Zn. Projector augmented-wave (PAW)^{36,37} theory combined with a plane-wave cutoff of 700 eV was used to describe the wave functions. The convergence threshold for the total energy was set to 1 × 10⁻⁸ eV, ensuring an accurate sampling of the complex potential energy surface of these MOFs. The structure of M(bdc)(ted)_{0.5} interacting with SO₂ was relaxed using vdW-DF until the force criterion of 1 × 10⁻⁴ eV·Å⁻¹ was satisfied. Experimentally, the Zn(bdc)(ted)_{0.5} structure exhibits some proton statistical disorder (previously studied by Kong et al.³⁸) resulting in a tetragonal cell with *a*, *b* = 10.93 Å, and *c* = 9.61 Å.

The Ni(bdc)(ted)_{0.5} structure was obtained after full relaxation of the Zn(bdc)(ted)_{0.5} where Zn atoms were replaced by Ni atoms. The optimized lattice constants for Ni(bdc)(ted)_{0.5} are *a* = *b* = 11.15 Å and *c* = 9.53 Å, respectively. For Ni(bdc)(ted)_{0.5} the magnetic moment exhibited by the Ni atoms (2 per cell) is approximately 1 μB per Ni atom and remains entirely localized on the Ni species.

With these settings, we fully relaxed the coordinates of the MOF and the adsorbed species, for which the adsorption energies are calculated. Starting from the well-converged adsorption geometries, we simulated the IR/Raman vibrational modes of SO₂. Vibrational frequencies were obtained by diagonalizing the dynamical matrix at the Γ point using a finite difference approach with a three-point formula and a calibrated displacement of 0.005 Å. Bader charges were computed using the fast implementation of Henkelman and co-workers.³⁹ The adsorption models and the graphic manipulation were carried out using J-ICE.⁴⁰

3. EXPERIMENTAL RESULTS

3.1. Adsorption Isotherms. The M(bdc)(ted)_{0.5} series contains secondary-building units SBUs of two 5-coordinates metal cations bridged in a paddle wheel-type configuration (see Figure 1).^{41–44} Compared to the MOFs with coordinatively unsaturated metal sites, M(bdc)(ted)_{0.5} is more readily activated and highly porous (61.3%) with large BET surface areas exceeding 1700 m²/g.^{44,45}

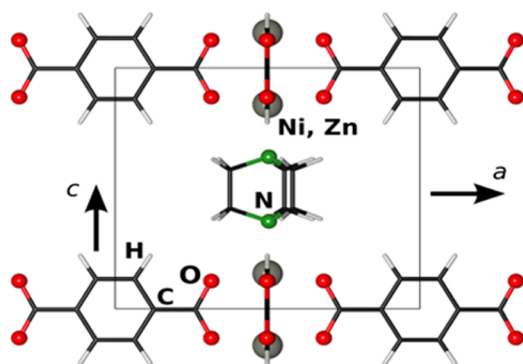


Figure 1. Structure of $M(\text{bdc})(\text{ted})_{0.5}$ ($M = \text{Ni}$ and Zn) viewed along the a and c axes. Each paddle wheel building unit is linked by bdc within the layer of 2D network (xy plane). The apical sites of metal ions in the building units are bonded by ted molecules to generate the 3D porous frameworks. The coordinative bonds between metal ions Ni^{2+} , Zn^{2+} and O, N atoms of bdc , ted linkers are omitted.

The SO_2 adsorption isotherms for activated $\text{Ni}(\text{bdc})(\text{ted})_{0.5}$ and $\text{Zn}(\text{bdc})(\text{ted})_{0.5}$ were collected at 298 K. The data are shown in Figure 2. For the pressures below 0.35 bar, the SO_2 uptake in $\text{Ni}(\text{bdc})(\text{ted})_{0.5}$

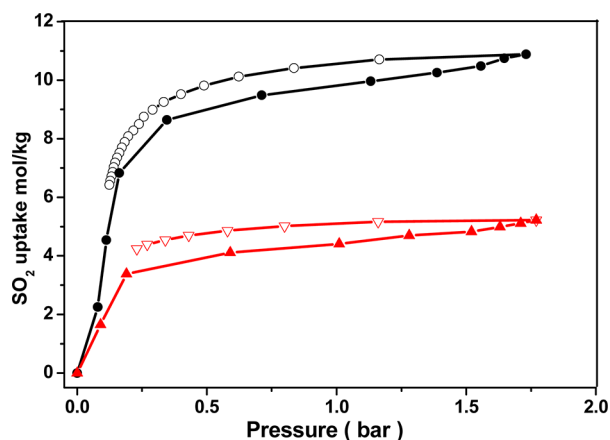


Figure 2. Adsorption isotherm of SO_2 in $\text{Ni}(\text{bdc})(\text{ted})_{0.5}$ (black), $\text{Zn}(\text{bdc})(\text{ted})_{0.5}$ (red) at room temperature for pressures up to ~ 1.8 bar. Solid symbol: adsorption. Empty symbol: desorption.

increases rapidly to 8.64 mol/kg, and then reaches 10.88 mol/kg at 1.73 bar. This is quite similar to the SO_2 isotherms observed in NOTT-300.²⁴ The rapid increase observed can be attributed to the strong interaction of SO_2 with the surface of the frameworks determined by spectroscopic measurements and theoretical calculations in a later section. Table 1 shows that at room temperature and around 1 bar, $\text{Ni}(\text{bdc})(\text{ted})_{0.5}$ outperforms the other reported metal organic frameworks materials in SO_2 adsorption with 9.97 mol/kg SO_2 uptake capacity, compared for instance with Mg-MOF-74, as previously shown in breakthrough measurements, found here under isotherm conditions to have 8.60 mol/kg SO_2 uptake capacity. In contrast, at low pressure (< 0.20 bar), MOF-74 and NOTT-300 adsorb more SO_2 than $\text{Ni}(\text{bdc})(\text{ted})_{0.5}$. Comparing the uptake of different gases (CO_2 , N_2 , CH_4 , H_2),^{44,46,47} as shown in Supporting Information Table S2 and coadsorption measurement in Supporting Information, it is found that $\text{Ni}(\text{bdc})(\text{ted})_{0.5}$ exhibits a preferential adsorption toward SO_2 . The observed hysteresis during the desorption process is attributed to kinetic limitations. The SO_2 adsorption uptake in the isostructural $\text{Zn}(\text{bdc})(\text{ted})_{0.5}$ compound is much lower than in $\text{Ni}(\text{bdc})(\text{ted})_{0.5}$, which can be explained by the stability of $M(\text{bdc})(\text{ted})_{0.5}$ [$M = \text{Ni}$, Zn] under SO_2 . The XRD pattern (see Supporting Information Figure S3) reveals that that the crystal structure of $\text{Ni}(\text{bdc})(\text{ted})_{0.5}$ is stable under SO_2 loading while that of $\text{Zn}(\text{bdc})$ -

Table 1. Comparison of SO_2 Adsorption Capacities (Uptakes in mol kg^{-1}) in Selected MOF at Room Temperature

MOF	uptake	pressure (bar)	temp. (K)	reference
$\text{Ni}(\text{bdc})(\text{ted})_{0.5}$	9.97	1.13	298	this work
$\text{Zn}(\text{bdc})(\text{ted})_{0.5}$	4.54	0.11	298	this work
Mg-MOF-74	8.60	1.02	298	this work
	6.44	0.11	298	this work
	1.94	a	293	21
NOTT-300	8.1	1	273	24
$\text{M}_3[\text{Co}(\text{CN})_6]_2$	2.5	1	298	13
FMOF-2	2.19	1	298	12

^aThe dynamic capacity of SO_2 in Mg-MOF-74 measured by breakthrough measurement under 1000 mg m^{-3} of the feed concentration.

(ted)_{0.5} shows evidence of partial decomposition. The high thermal stability of $\text{Ni}(\text{bdc})(\text{ted})_{0.5}$ (over $400 \text{ }^\circ\text{C}$ as shown in Supporting Information Figure S4) makes it suitable for real world applications.

3.2. Spectroscopic Characterization of SO_2 Adsorption and Desorption in $M(\text{bdc})(\text{ted})_{0.5}$. To unravel the nature of the interactions between SO_2 molecules and the $\text{Ni}(\text{bdc})(\text{ted})_{0.5}$ framework upon SO_2 adsorption, we performed *in situ* IR measurements of SO_2 adsorption at room temperature as a function of pressure. Since the SO_2 gas IR absorption at pressures above 100 Torr is prohibitively high, a different procedure was employed to study the loadings above 45 Torr (see Supporting Information Figure S6). The activated sample was exposed to the SO_2 gas and the pressure cell quickly evacuated. The IR spectra were then recorded immediately after evacuation (acquisition time = 16 s). The adsorption state could be probed because the kinetics of SO_2 removal are slow enough, as shown in Figure 3. Several SO_2 associated bands, increasing as a function of initial pressure, can be identified in the IR spectra for $\text{Zn}(\text{bdc})(\text{ted})_{0.5}$ of Figure 3 and Supporting Information Figure S7. Two sharp bands observed at 1326 cm^{-1} and 1144 cm^{-1} , exhibit a -36 cm^{-1} and -7 cm^{-1} red-shift, respectively (from the unperturbed values of 1362 cm^{-1} and 1151 cm^{-1} for the asymmetric and symmetric S=O stretch modes of SO_2 molecules).^{48–50} Although these frequency shifts are

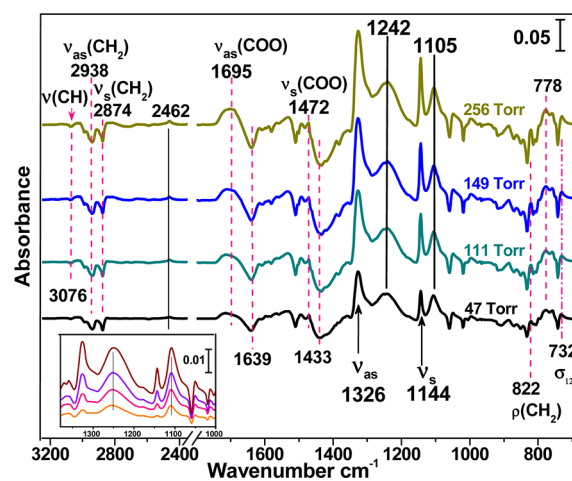


Figure 3. IR absorption spectra of SO_2 adsorption into $\text{Ni}(\text{bdc})(\text{ted})_{0.5}$ as a function of SO_2 initial pressure recorded immediately after evacuation (within 16 s). All spectra are referenced to the activated (i.e., empty) MOF. Inset shows the low pressure region from bottom to top: 600 mtor, 1 Torr, 2 Torr, 3 Torr. The black lines are associated with SO_2 -related features and the red dash lines with MOF-related features arising from SO_2 induced perturbation.

typical of physisorbed SO_2 species,^{49,51} we will show in section 4.1 that there can be charge transfer with the MOF.

A combination band, $\nu_{\text{as}}+\nu_{\text{s}}$, is observed at 2462 cm^{-1} . Two other bands appear at 1242 cm^{-1} and 1105 cm^{-1} , most easily seen in the low pressure range (see inset of Figure 3), which are substantially more red-shifted compared to the gas phase values (-120 and -53 cm^{-1} , respectively) than these of the previous bands discussed above. SO_2 adsorption also induces significant changes to the frameworks vibrational modes: (1) a blue shift of the $\nu_{\text{as}}(\text{COO})$ mode from 1639 cm^{-1} to 1695 cm^{-1} ($\Delta\nu = +56\text{ cm}^{-1}$) and of the $\nu_{\text{s}}(\text{COO})$ mode from 1433 cm^{-1} to 1472 cm^{-1} ($\Delta\nu = +39\text{ cm}^{-1}$), and (2) a decrease in intensity of $\nu_{\text{as}}(\text{CH}_2)$, $\nu_{\text{s}}(\text{CH}_2)$ and $\nu(\text{CH})$ modes at 2874 cm^{-1} , 2938 cm^{-1} , and 3076 cm^{-1} , respectively. Furthermore, the CH_2 rocking mode and benzene ring deformation mode σ_{12} are red-shifted by $\sim -8\text{ cm}^{-1}$ (from 830 and to 822 cm^{-1}) and $\sim -12\text{ cm}^{-1}$ (from 744 cm^{-1} to 732 cm^{-1} , respectively). The $\delta(\text{COO})$ mode, initially at 810 cm^{-1} shifts to 778 cm^{-1} ($\Delta\nu = -32\text{ cm}^{-1}$). These changes increase with SO_2 adsorption. The frameworks vibrational modes assignment is summarized in Supporting Information Table S3.

Figure 4 shows the evolution of SO_2 in $\text{Ni}(\text{bdc})(\text{ted})_{0.5}$ after a loading at 286 Torr . Upon evacuation at room temperature, the

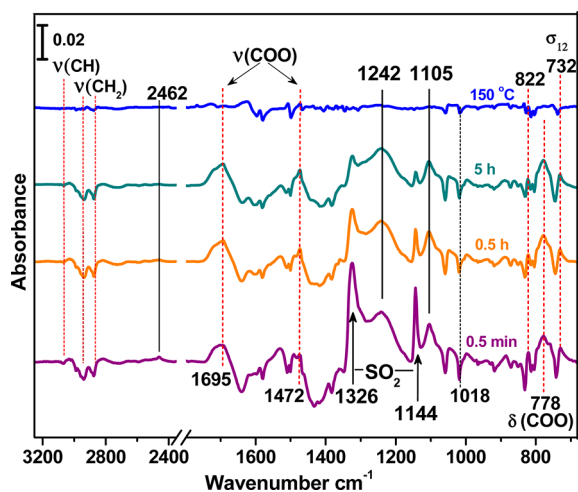


Figure 4. IR absorption spectra recorded 0.5 min, 0.5 h, and 5 h after evacuation at room temperature after loading SO_2 at 286 Torr , and then after at $150\text{ }^\circ\text{C}$ for additional 3 h. All spectra are referenced to the activated (i.e., empty) MOF. The vertical black lines are associated with SO_2 -related features and the red dash or dot lines with MOF-related features arising from SO_2 -induced perturbations.

physisorbed species characterized by modes at 1326 cm^{-1} and 1144 cm^{-1} gradually desorbs. In contrast, the two bands at 1242 cm^{-1} and 1105 cm^{-1} remain relatively strong, indicating that another more strongly bound SO_2 species is present in the frameworks.

In coadsorption experiments of CO_2 and SO_2 in Supporting Information Figure S9, we found that the presence of this other SO_2 species can decrease the CO_2 adsorption. The complete removal of this species required heating to $150\text{ }^\circ\text{C}$, as shown in the top spectrum in Figure 4. In the differential spectra, the perturbed benzene ring stretching bands ν_{18a} , ν_{19b} , ν_{19a} modes, benzene ring deformation modes σ_{12} , $\nu(\text{COO})$, $\rho(\text{CH}_2)$ of ted linkers are partially recovered after the removal of the dominant, less strongly bound SO_2 molecules upon evacuation at room temperature. Comparison of Figures 4 and 5 indicates that the weakly bound SO_2 (characterized by modes at 1326 cm^{-1} and 1144 cm^{-1}) causes the σ_{12} mode to blue shift by 4 cm^{-1} while the more strongly bound SO_2 characterized by modes at 1242 cm^{-1} and 1105 cm^{-1} causes the σ_{12} mode red shift to 732 cm^{-1} . The perturbation of the $\nu(\text{COO})$, $\nu(\text{CH}_2)$, $\delta(\text{COO})$ bands, and the benzene deformation mode σ_{12} are removed after this latter species, characterized by modes at 1242 cm^{-1} and 1105 cm^{-1} , has desorbed at elevated temperatures.

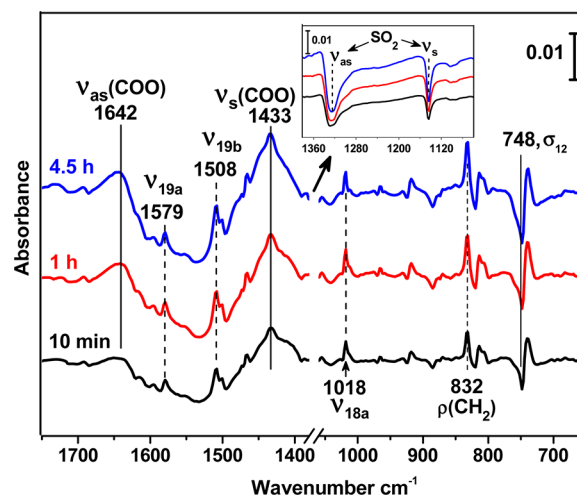


Figure 5. Differential spectra recorded during evacuation. The reference for all spectra is obtained at the very beginning of the evacuation process (i.e., within 0.5 min). The inset shows the physisorbed SO_2 in the frequency region of 1050 to 1380 cm^{-1} .

3.3. Perturbation with D_2O , SO_2 , and CO_2 . To elucidate the nature of the perturbation of the MOF structure (i.e., phonons), we examined the effect of adsorption of other molecules (water and carbon dioxide) into the $\text{Ni}(\text{bdc})(\text{ted})_{0.5}$ frameworks on the IR absorption spectra (Figure 6). For water, D_2O is used instead of H_2O

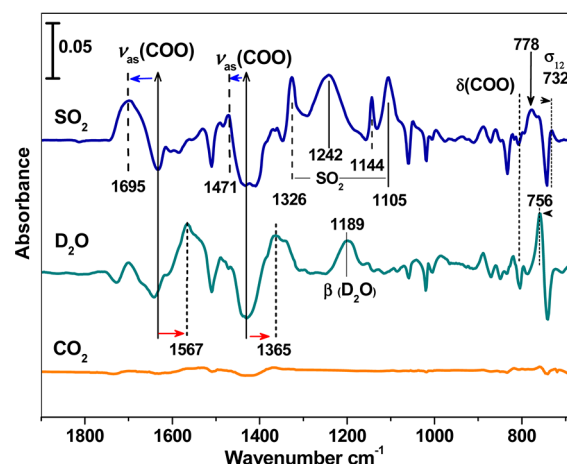


Figure 6. Perturbation of MOFs vibrational modes: IR absorption spectra of SO_2 , D_2O , CO_2 adsorption into $\text{Ni}(\text{bdc})(\text{ted})_{0.5}$ recorded right after exposure following (a) 16 Torr SO_2 , (b) $6\text{ Torr D}_2\text{O}$, and (c) 16 Torr CO_2 . All spectra are referenced to the activated (i.e., empty) MOF.

to avoid the interference of the $\beta(\text{D}_2\text{O})$ (scissor) mode in the range 1600 – 1700 cm^{-1} . We find that the perturbation effect induced by SO_2 adsorption is significantly different from incorporation of water molecules into the $\text{M}(\text{bdc})(\text{ted})_{0.5}$ frameworks and it is dependent on the adsorbed species. As previously observed and discussed,³⁵ the $\nu_{\text{as}}(\text{COO})$ and $\nu_{\text{s}}(\text{COO})$ modes, initially at $\sim 1620\text{ cm}^{-1}$ and $\sim 1430\text{ cm}^{-1}$, red shift to 1567 cm^{-1} and 1365 cm^{-1} upon introduction of the water molecules. The red shift is due to hydrogen bonding between D_2O and the carboxylate group in the paddlewheel building units. In the case of CO_2 , there is little perturbation of the host, which is consistent with the fact that CO_2 is known to be weakly physically adsorbed into $\text{M}(\text{bdc})(\text{ted})_{0.5}$.⁵¹ The response of the benzene ring deformation mode σ_{12} , $\delta(\text{COO})$, is specific to each guest-molecule adsorption into the frameworks: σ_{12} blue shift to 756 cm^{-1} upon

exposure to water vapors; SO₂ adsorption causes a more pronounced red shift of the $\delta(\text{COO})$ mode than water molecules.

4. DISCUSSION

The infrared results indicate that SO₂ adsorbs into the M(bdc)(ted)_{0.5} frameworks in two different ways, distinguished by their frequency shifts, effect on the host spectrum and bonding strengths. From the desorption isotherms shown in Figure 2 and the IR absorption spectra in Figure 4, we conclude that the major species is weakly adsorbed SO₂, characterized by modes at 1326 cm⁻¹ and 1144 cm⁻¹. In addition, we observe that some minor species persists in the framework upon evacuation and can block access to other molecules such as CO₂ as indicated in Figure 4 and Supporting Information Figure S9. Upon the removal of this more strongly bound SO₂ species, the CO₂ uptake can be recovered, confirming that these SO₂ species inhibit the adsorption of incoming CO₂ molecules.

To determine the origin of all adsorbed species, we first turn to the literature. Previous experimental and theoretical studies of SO₂ interaction with metal oxide such as MgO and ZnO suggest that SO₂ readily reacts with exposed O sites at surfaces to form SO₃ and in some cases SO₄ species.^{52–54} According to this picture, it is likely that SO₂ molecules preferentially interact with the oxygen site of the paddlewheel building units by Lewis acid–base interaction. For such an interaction, perturbations of the $\nu_s(\text{COO})$ bands are expected, as observed in the IR spectra (see section 3.2). However, other sites may also be occupied leading to other types of interactions. For instance, the “strong” perturbations of the linker bands such as $\nu(\text{CH}_x)$, ν_{18a} , $\rho(\text{CH}_2)$, and σ_{12} indicate the possible interaction of SO₂ molecules with the benzene rings and the ted moieties in the frameworks as well.

While the modes associated with the dominant species at 1326 cm⁻¹ and 1144 cm⁻¹ correspond to physisorbed SO₂ according to the isotherms, the other two bands at 1242 cm⁻¹ and 1105 cm⁻¹ are clearly associated with more strongly bound SO₂ species, with frequencies more similar to previously observed values for sulfate species and chemisorbed SO₃ on MgO surfaces.^{50,55,56} It would therefore be tempting to suggest that SO₂ is oxidized into SO₄ species within the Ni(bdc)(ted)_{0.5} framework by a so-called $\eta^1\text{-S}$ bridge configuration,^{52,54,56} wherein SO₂ is attached via the S atom to two oxygen atoms of the paddle wheel building units (Lewis adduct formation), as shown in Supporting Information Figure S11. However, the spectroscopic results in Figure 3 and 4 suggest that SO₂ interacts instead the ted organic linker since the appearance of the bands at 1242 and 1105 cm⁻¹ is correlated with a decrease in intensity of $\nu_{as}(\text{CH}_2)$, $\nu_s(\text{CH}_2)$ modes of the ted group.

To determine whether this interaction involves the ted group, two other isotypical metal organic frameworks without ted linker, but based on the same paddlewheel building units, Zn(ndc)(bpee)_{0.5} and Zn(ndc)(bpy)_{0.5} were studied, where [ndc = 2,6-naphthalenedicarboxylate, bpee = 1,2-bis(4-pyridyl) ethylene, and bpy = bipyridine] (see Figure 7).^{57,58} For these MOFs, bpee and bpy link the two-dimensional networks Zn₂(ndc)₂ to generate 3D pillared structures similar to Zn(bdc)(ted)_{0.5}. Since the bpy and bpee linkers are planar linkers in contrast to the 3-D ted linker, there should be less steric hindrance for SO₂ molecules to interact with the paddlewheel units, if the formation of a Lewis carboxylate-SO₂ bonding were in fact stable, in Zn(ndc)(bpee)_{0.5}, and Zn(ndc)(bpy)_{0.5}. Importantly, no feature associated with

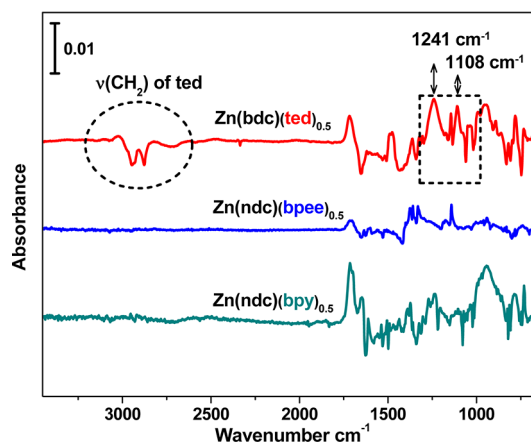


Figure 7. IR absorption spectra of SO₂ adsorption into activated Zn(bdc)(ted)_{0.5}, Zn(ndc)(bpee)_{0.5}, and Zn(ndc)(bpy)_{0.5} at the pressure of 23 Torr, 20 Torr, 24 Torr recorded immediately after evacuation (within 16 s). All spectra are referenced to the activated (i.e., empty) MOF.

strongly bound species were observed in the spectra of SO₂-loaded Zn(ndc)(bpee)_{0.5} and Zn(ndc)(bpy)_{0.5}, ruling out the formation of SO₄ type species (with O–O distance ~2.4–2.5 Å) in paddlewheel units, possibly due to large O–O distances (~2.7–2.8 Å) in the carboxylate groups of the unit.^{41,42,59}

These results suggest that the interaction with the ted linker may be strong enough to induce the shifts observed in the SO₂ vibrational spectrum, 1242 and 1105 cm⁻¹, and to lead to a higher binding energy, as shown in Figure 4 and Figure 7. We have therefore examined such possibilities using first principles calculations that are useful to determine the binding energies associated with selected binding sites of SO₂ molecules within the Ni/Zn(bdc)(ted)_{0.5} and to calculate the associated vibrational spectrum of both SO₂ and the MOF ligand modes, as described in section 4.1.

Ni/Zn(bdc)(ted)_{0.5} offer several potential binding sites associated with the nature of their building block. However, their potential energy surface (PES) is complex, presenting many adsorptions “pockets”. To guide the construction of initial and realistic adsorption geometries, we initially assumed that the interaction of SO₂ with MOFs structure was similar to what occurs when SO₂ is adsorbed on simpler systems such MgO and ZnO surfaces.^{52,54} This assumption is justified by the fact that oxygen atoms surrounding the metals sites of MOFs M(bdc)(ted)_{0.5} “recreate” the chemical environment found on these surfaces. Theoretical and experimental evidence of the adsorption of SO₂ on MgO and ZnO surfaces suggests that SO₂ interacts strongly with its sulfur atom with the oxygen sites exposed at the surface, leading us to design an initial model of interaction where the sulfur atoms of SO₂ bind with the oxygen atoms of the bdc units (model SO₂–O–bdc). However, due to the complexity of PES of the M(bdc)(ted)_{0.5}, we also considered three other possible initial adsorption sites, based on the complementarity electrostatic principle of Lewis-donors and acceptors. In general, S in SO₂ acts as an acceptor, and the functionalities on the linker as the donors. This has led us to select adsorption geometries (i.e., models) where SO₂ is in contact with (i) the benzene ring of the bcd units (model SO₂-benzene), (ii) with the nitrogen atom of the ted group (model SO₂-N-ted), and (iii) the C–H groups of the ted linkers by establishing strong hydrogen bond (SO–H–C) with several

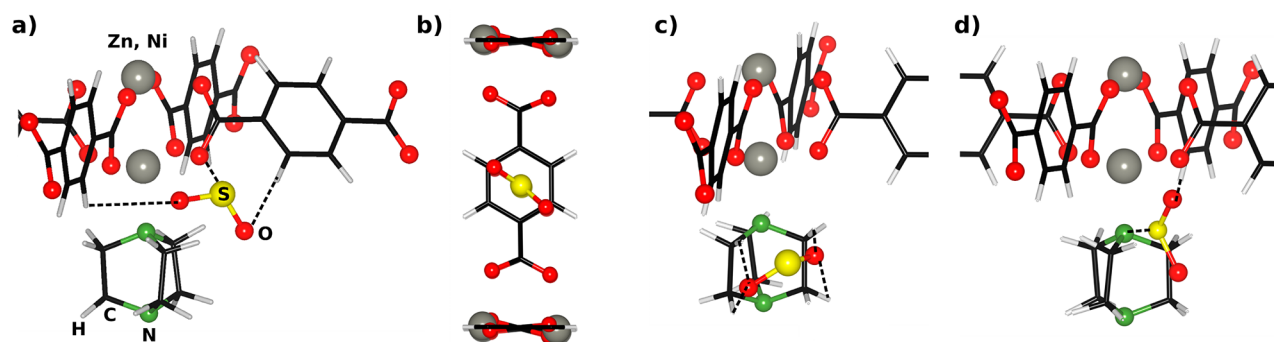


Figure 8. Snapshot of four initial adsorption configuration models used to investigate possible interactions of SO_2 in $\text{Zn, Ni(bdc)(ted)}_{0.5}$. (a) $\text{SO}_2\text{-O-bdc}$, (b) $\text{SO}_2\text{-benzene}$, (c) $\text{SO}_2\text{-CH}_2\text{-ted}$, and (d) $\text{SO}_2\text{-N-ted}$. Dashed lines represent the shorter contacts for SO_2 with the surrounding groups available on the linker unit.

such C–H groups that are fully accessible in the MOF channel of the model $\text{SO}_2\text{-CH}_2\text{-ted}$ system.

4.1. Adsorption Energy and Charge Analysis. The fundamental quantity that governs the adsorption properties of SO_2 within the MOF is the adsorption energy ΔE , referred to thereafter as binding energy:

$$\Delta E = E_{\text{MOF}+\text{G}} - E_{\text{MOF}} - E_{\text{G}} \quad (1)$$

Here, $E_{\text{MOF}+\text{G}}$, E_{MOF} , and E_{G} are the total energies of the fully relaxed MOF + SO_2 , MOF alone, and SO_2 in gas phase, respectively. Knowledge of the vibrational frequencies (section 4.2) of these systems becomes useful in the calculation of the zero-point energy (ZPE), ΔE_{ZPE} , the thermal correction $\Delta H(T)$, and entropy contribution ΔS . $\Delta H(T)$ allows for a more accurate comparison to measured heats of adsorption and is calculated considering the vibrational contribution (taking into account the rotational and translational degrees of freedom for the molecule in gas phase) to the adsorption energy.

We begin by discussing the binding energies and other relevant quantities for monoadsorption cases of SO_2 molecules within $\text{Zn(bdc)(ted)}_{0.5}$ framework as detailed above, and Figure 8 shows these initial alternative adsorption models.

The adsorption of SO_2 molecules on the groups presented by the MOF follow the trend: $\text{SO}_2\text{-N-ted}$ (-5 kJ mol^{-1}) > $\text{SO}_2\text{-benzene}$ (-22 kJ mol^{-1}) > $\text{SO}_2\text{-CH}_2\text{-ted}$ (-61 kJ mol^{-1}) \geq $\text{SO}_2\text{-O-bdc}$ (-66 kJ mol^{-1}).

The initial configuration of SO_2 interacting with the nitrogen atom of the ted group evolves quite dramatically during the structural optimization, resulting in the complete desorption of the SO_2 molecule from the ted unit back into the MOF channel. The small adsorption energy observed (-5 kJ mol^{-1}) originates from the weak interactions of SO_2 with the surrounding linker groups rather than with N. This situation has been expected since the cramped chemical environment of the ted group, and specifically the poor accessibility to the N atoms from the MOF-channel (see Figure 8d).

The model of the SO_2 molecule on the benzene site was investigated by both calculations (see section S11 in the Supporting Information) and the experimental work of Taleb-Bendiab et al.,⁶⁰ which show that the binding energy for this configuration is $\Delta E_{\text{b}}(\text{theory}) = -22 \text{ kJ mol}^{-1}$ and $\Delta E_{\text{b}}(\text{exp}) = -18 \text{ kJ mol}^{-1}$, respectively, that is, much less than for SO_2 in the other configurations $\text{SO}_2\text{-CH}_2\text{-ted}$ and $\text{SO}_2\text{-O-bdc}$. Note that the calculations were done for $\text{Zn(bdc)(ted)}_{0.5}$, but very similar results are expected for the iso-structural $\text{Ni(bdc)(ted)}_{0.5}$, since the bonding does not involve the metal ions.

The Bader charge analysis of Table 2 suggests that in the cases of $\text{SO}_2\text{-O-bdc}$ and $\text{SO}_2\text{-benzene}$, the sulfur atom of

Table 2. Bader Charges (in Units of the Electronic Charge) of Sulfur in SO_2 and the Adsorbing Group (Grp) before (as B) and after (as A) the Adsorption^a

model	SO_2			Grp	MOF-atom		
	B	A	$\Delta\epsilon$		B	A	$\Delta\epsilon$
–O– bdc	+2.85	+1.73	–1.11	O	–1.19	–1.08	0.10
–CH ₂ – ted	+2.85	+2.07	–0.79	H ^b	–0.06	–0.09	–0.03
–benz.	+2.85	+2.72	–0.14	C ^c	0.05	0.05	0.00

^a $\Delta\epsilon$ is the absolute difference between charges. ^b SO_2 is pointing with its oxygen atoms on H atoms of the $\text{CH}_2\text{-ted}$ group see Figure 8c. ^cThe charges on carbon atoms of the benzene were averaged.

SO_2 always acts as acceptor, while the MOF-unit groups (i.e., benzene, or O) act as donors. This situation changes for the $\text{SO}_2\text{-CH}_2\text{-ted}$ model where the hydrogen bonds are between O atoms of the SO_2 molecule and the H atoms of the CH_2 group of the ted unit (see Figure 8c).

The charge analysis of Table 2 shows that the “charge transfer” from the MOF toward the SO_2 molecule is correlated with the adsorption energy by assisting the electron-deficiency of sulfur. For instance, the sulfur atom in the $\text{SO}_2\text{-O-bdc}$ and $\text{SO}_2\text{-CH}_2\text{-ted}$ configurations almost changes its oxidation state during adsorption on the oxygen atom of the bdc group, suggesting a bonding mechanism stronger than typical physisorption. However, the binding energy (-66 kJ mol^{-1}) is still in the range that is typically associated with physical adsorption. In contrast, SO_2 adsorption on the benzene rings leads to a small variation in the molecule and MOF charges, a clear indication of a weak van der Waals interaction that is consistent with lower calculated binding energy (-22 kJ mol^{-1}) and the shallow binding energy profile (see section S11 in the Supporting Information). Note that the Bader analysis is an intuitive (but not unique) way of repartitioning the electron charge density, similar to other charge analyses and therefore can only be used to draw qualitative conclusions.⁶¹

Initially, we postulated that the strongly bound species, characterized by the modes at 1242 and 1105 cm^{-1} in Figures 3, 4, and 5, could be associated with the geometry shown in Figure 8c with SO_2 located next to the ted CH_2 group. However, the binding energy calculated from the $\text{SO}_2\text{-CH}_2\text{-ted}$ model (-61 kJ mol^{-1}) is too low, even slightly less than

that of the $\text{SO}_2\text{-O-bdc}$ model in Figure 8a, which is not consistent with the measured elevated desorption temperature (150 °C). The frequencies of ν_{as} and ν_{s} mode of SO_2 molecules in this configuration also exhibit a modest red-shift of -31 and -20 cm^{-1} , much less than the observed frequency shifts of the strongly bound species (see section 4.2). Therefore, the theoretical calculations cannot shed light on the binding configuration of the strongly bound SO_2 . The spectroscopic results in Figure 7 clearly show that this adsorption state is associated with the ted linker because its CH_2 stretching modes are significantly perturbed. Interestingly, the inclusion of this strongly bound species brings in significant modifications to carboxylate and CH_x vibrational modes of the MOF (as shown in section 3.2, section 3, and Supporting Information Figure S8). Further extensive additional theoretical and experimental studies necessary to fully understand this interaction are beyond the scope of this work. They will involve the preparation of more isotypical MOFs containing ted linkers, which is important to explore more binding geometries with different expected SO_2 interactions with the ted group.

In order to fully investigate the loading capabilities of $\text{M}(\text{bdc})(\text{ted})_{0.5}$ and the MOF structure perturbation, we have progressively adsorbed an increasing number of SO_2 molecules (1–8 molecules) until the available oxygen atoms are completely saturated. Here, we explore the effect of loading only for the most stable adsorption case, that is, $\text{SO}_2\text{-O-bdc}$ and $\text{SO}_2\text{-CH}_2\text{-ted}$. The MOF $\text{Zn}(\text{bdc})(\text{ted})_{0.5}$ structure displays 8 oxygen atoms originating from bdc linkers (see red atoms at the center of Figure 8b). In Table 3, we report the

Table 3. Adsorption Energies ΔE (in kJ mol^{-1}) of SO_2 in Zn, Ni $(\text{bdc})(\text{ted})_{0.5}$ ^a

loading	ΔE	ΔE_{ZPE}	ΔH_{298}	ΔS	S–O*	$\Delta\phi$
Model $\text{SO}_2\text{-CH}_2\text{-ted Zn}(\text{bdc})(\text{ted})_{0.5}$						
1/8	-61	-58	-68	-218	2.56 ^b	
Model $\text{SO}_2\text{-O-bdc Zn}(\text{bdc})(\text{ted})_{0.5}$						
1/8	-66	-64	-70	-220	2.84	-43
2/8	-66	-62	-68	-223	2.87	-40
4/8	-66	-64	-70	-221	2.99	-44
6/8	-71	-69	-75	-226	3.07	-48
8/8	-78	-71	-77	-227	3.16	-49
Model $\text{SO}_2\text{-O-bdc Ni}(\text{bdc})(\text{ted})_{0.5}$						
2/8	-77	-75	-81	-228	2.90	-46

^a ΔE is also corrected by the ZPE and thermal contribution ΔH at 298 K. Entropies, $\Delta S\text{ J mol}^{-1}\text{ K}^{-1}$, are also reported. For the $\text{SO}_2\text{-O-bdc}$ model S–O is the averaged intermolecular bond-length OOS–O–(bdc) in Å, whereas $\Delta\phi$ is the variation of the torsion angle, in degrees, shown in Figure 8. ^bS–O bond length becomes O–H for $\text{SO}_2\text{-CH}_2\text{-ted}$ model (see Figure 8c).

adsorption energies (with relative contribution) along with relevant bond-lengths and structural parameters of the most relevant adsorption geometries, that is, $\text{SO}_2\text{-O-bdc}$ and $\text{SO}_2\text{-CH}_2\text{-ted}$.

Table 3 shows that SO_2 binds strongly with the oxygen atoms in the Ni and $\text{Zn}(\text{bdc})(\text{ted})_{0.5}$ structures, which is expected to affect the frequencies of $\nu(\text{COO})$ modes as observed in Figure 5. Figure 9 highlights the limited configurations surrounding the metal sites in $\text{M}(\text{bdc})(\text{ted})_{0.5}$ available for SO_2 adsorption. Figure 9 also shows the formation of hydrogen bonds between the oxygen atoms of SO_2 and the hydrogen on the benzene ring of the linkers. The magnitude of

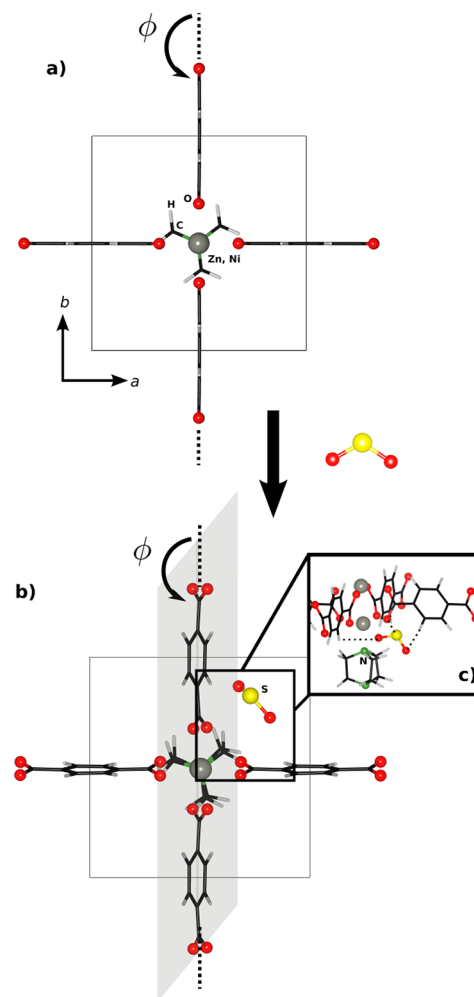


Figure 9. Top-view of $\text{M}(\text{bdc})(\text{ted})_{0.5}$ (a) before and (b) after the absorption of SO_2 molecules. (c) Enlargement of the adsorption area for SO_2 , where dashed lines show the interaction of S with O atoms (see bond length S–O in Table 2) of the MOF and hydrogen bonds. The structural deformation upon SO_2 absorption is highlighted by the gray plane in a, b, and ϕ is the torsion angle.

the distortion imposed by SO_2 on the MOF structure can be monitored by following the variation of the angle ϕ of Table 3. The large distortion imposes dramatic changes in the linker structure, affecting their vibrational frequencies as observed experimentally in the ring deformation mode σ_{12} and other ring stretching mode ν_{18a} , ν_{19b} , ν_{19a} shift in Figure 5.

In Figure 8c, SO_2 also forms hydrogen bonds with the CH_2 group of the ted linker through its two oxygen atoms, as evidenced by the close distance (2.56 Å) between O and H atoms shown in Figure 8c and Table 3. This is an interesting binding geometry since the ted linkers provide a chelating site for the guest SO_2 molecules. The experimentally observed perturbation of the $\rho(\text{CH}_2)$ mode shown in Figure 5 are consistent with the interaction between SO_2 and CH_2 (see section 3.2).

The calculated adsorption energies are large for $\text{M}(\text{bdc})(\text{ted})_{0.5}$, and they increase with loading. However, the calculated decrease of ΔE with the molecular loading could be an artifact of the increasing intermolecular interactions, caused by the finite size of the cell adopted. For such reasons, our analysis of the absorption of SO_2 in $\text{Ni}(\text{bdc})(\text{ted})_{0.5}$ is only restricted to a representative model for two SO_2 per unit cell

(2/8). The binding energies for this latter MOF are similar to those of Zn(bdc)(ted)_{0.5}.

The above adsorption energy calculations, combined with the later IR frequencies simulation, suggest that the infrared bands at 1326 and 1144 cm⁻¹ species could be due to SO₂ trapped in either SO₂-CH₂-ted or SO₂-O-bdc configurations since their adsorption energies and IR frequency shift as calculated in the next section are similar. The observation that the benzene ring deformation modes σ_{12} and stretching modes of ν_{18a} , ν_{19b} , ν_{19a} are affected by this weakly bound SO₂ additionally confirms the existence of the second configuration (SO₂-O-bdc) shown in Figure 8a.

4.2. Simulation of IR Spectra. We further discuss the effect of adsorption on the IR frequency modes of SO₂. The theoretical analysis concerns the vibrational modes of SO₂ and the MOF in gas-phase and once adsorbed into M(bdc)(ted)_{0.5} (M = Zn, Ni), respectively, as reported in Table 4. The

Table 4. Simulated IR Vibrational Frequencies (in cm⁻¹) for SO₂ in Gas-Phase and Within M(bdc)(ted)_{0.5} (M = Ni, Zn)^a

SO ₂ -gas			M(bdc)(ted) _{0.5}		
exp.	cal.	Ni	Zn (SO ₂ -O-bdc)	Zn (SO ₂ -CH ₂ -ted)	
ν_{as}	1362 ^b	1256	1217 (-39)	1224 (-32)	1225 (-31)
ν_s	1151 ^b	1073	1053 (-20)	1057 (-16)	1053 (-20)
δ	497 ^c	498	491 (-7)	501 (+3)	497 (-1)

^aExperimental frequencies value for the SO₂ gas-phase are also reported. In brackets, we report the frequency shifts with respect to those calculated for the gas-phase. ^bThis work (see section 3.2). ^cRef 62.

frequency calculations presented here are only performed for specific configurations: 2 SO₂/8 sites of loading for M(bdc)(ted)_{0.5} (M = Zn, Ni) (see Table 2). The analysis focuses initially on the SO₂ frequency shifts observed when the first molecule is introduced in the MOF channel. According to the irreducible representation of SO₂, C_{2v}, there are three expected vibrational modes: that is, two stretching modes (asymmetric and symmetric) and one bending mode.

From Table 4, it is clear that the computed IR frequencies of the SO₂ gas-phase are underestimated. To determine if such a discrepancy is due to the pseudopotential (PS) employed, we performed a similar calculation using a "harder" PS, which increases the computational cost, but we observed only a marginal change of the absolute frequency values (about +20 cm⁻¹).

Nevertheless, the quantity of interest here is the frequency shift upon SO₂ adsorption within the MOF structure, which is more accurately determined than the absolute frequencies. Table 4 shows that the SO₂ vibrational modes experience a shift once in the M(bdc)(ted)_{0.5} structure. In both SO₂-O-bdc and SO₂-CH₂-ted configurations, the molecular adsorption leads to similar red-shifts of the stretching modes, ν_3 and ν_1 , as shown in Table 4, a clear indication that those bonds are weakened due to the SO₂ interaction with the MOF. The bending modes are not affected much after the adsorption of SO₂. Experimentally, for Ni(bdc)(ted)_{0.5}, two sharp bands are observed at 1326 cm⁻¹ and 1144 cm⁻¹, respectively, corresponding to \sim -36 cm⁻¹ and \sim -7 cm⁻¹ red-shifts (from the unperturbed value at 1362 cm⁻¹ and 1151 cm⁻¹) of the asymmetric and symmetric S=O stretch modes of the SO₂ molecules (see section 3.2). Although the absolute theoretical

values underestimate the values of the frequencies observed experimentally, the red shifts are in good agreement with the experimental measurements (see Table 4). As a guide for future interpretation, we report in Supporting Information Figure S14 the computed frequencies in form of the spectra, where only stretching modes are shown.

We also investigated the effect of the SO₂ adsorption on the vibrational modes of the MOF framework. Note that a full symmetry analysis of each mode associated with the MOF as well as a full description of each mode become extremely challenging; we therefore limit the discussion of Table 5 to the

Table 5. Simulated IR Vibrational Frequencies (in cm⁻¹) for SO₂ in Gas Phase and within Zn(bdc)(ted)_{0.5}^a

Zn(bdc)ted _{0.5}				
Grp	<i>m</i>	M(bdc)ted _{0.5}	SO ₂ -O-bdc	SO ₂ -CH ₂ -ted
CH (bdc)	ν	3053	3069 (+16)	3066 (+13)
CH ₂ (ted)	ν_{as}	3036	3040 (+4)	3043 (+7)
CH ₂ (ted)	ν_s	2996	3001 (+5)	3002 (+6)
COO(bdc)	ν_{as}	1549	1561 (+12)	1560 (+11)
COO(bdc)	δ	849	846 (-3)	848 (-1)
CH ₂ (ted)	ρ^b	821	829 (+8)	823 (+2)
COO(bdc)	δ_{oop}	788	788 (0)	789 (+1)
Ni(bdc)ted _{0.5}				
Grp	<i>m</i>	M(bdc)ted _{0.5}	SO ₂ -O-bdc	
CH(bdc)	ν	3050	3072 (+22)	
CH ₂ (ted)	ν_{as}	3030	3040 (+10)	
CH ₂ (ted)	ν_s	2988	2991 (+3)	
COO(bdc)	ν_{as}	1519	1530 (+11)	
COO(bdc)	δ	863	860 (-3)	
CH ₂ (ted)	ρ^b	829	835 (+6)	
COO(bdc)	δ_{oop}	777	778 (+1)	

^aIn brackets we report the frequency shifts with respect to those calculated for the bare MOF. Grp refers to the vibrating group, whereas *m* for modes. ^b ρ is the bending mode out of plane.

frequency modes that are detected experimentally (see section 3.2). Furthermore, the conclusions derived from the frequency calculations of the model SO₂-CH₂-ted segment of the Zn(bdc)(ted)_{0.5} framework are assumed to carry over for Ni(bdc)(ted)_{0.5} as well.

Table 5 shows that our calculations slightly overestimate the experimental CH stretching modes, while underestimate the COO asymmetric and symmetric frequencies (see section 3.2). In general, the shift of the calculated vibrational modes is quite small. Most of vibrational modes investigated are strongly affected both in intensity and peak position by the adsorption of a strongly bound species with modes at 1242 and 1105 cm⁻¹ (see section 3.2), making it difficult to analyze the measured peak position change induced by the more weakly adsorbed SO₂ (with modes at 1326 and 1144 cm⁻¹). The differential spectra in Figure 5 show that the perturbations of bdc and ted modes are partially released upon desorption of this more weakly bound species, providing indirect evidence for SO₂ interaction with the functional groups of organic linkers.

5. CONCLUSION

In this work, we have shown that the metal organic framework Ni(bdc)(ted)_{0.5} adsorbs a large quantity of polluting SO₂ gas [9.97 mol kg⁻¹] at 1.13 bar at room temperature. The high uptake capacity can be attributed to multiple interactions of

SO₂ molecules within the framework units. These include the interaction of sulfur atoms with paddlewheel metal oxygen carbon units of the secondary building unit and oxygen atoms of SO₂ with the C–H, CH₂ of organic linkers, as observed by infrared spectroscopy and supported by ab initio DFT calculations. The IR data also point to another configuration of SO₂ that is more strongly bound to the organic linker ted, and can be removed at higher temperature (~150 °C) without destroying the frameworks structure. These findings are important to develop frameworks based on paddlewheel building units for the efficient capture of SO₂.

■ ASSOCIATED CONTENT

■ Supporting Information

Mg-MOF-74 crystal structure and adsorption and desorption isotherm of SO₂, PXRD pattern of M(bdc)(ted)_{0.5} and TG profiles, Infrared spectra of Ni(bdc)(ted)_{0.5} and its vibrational assignments, different gas adsorption capacities in Ni(bdc)(ted)_{0.5}, IR spectra of SO₂ adsorption into Zn(bdc)(ted)_{0.5}. Co-adsorption experiment of CO₂ and SO₂, binding energy curve, and simulated IR spectra. This material is available free of charge via the Internet at <http://pubs.acs.org>.

■ AUTHOR INFORMATION

Corresponding Author

*Phone: 1-972-883-5751. E-mail: chabal@utdallas.edu.

Notes

The authors declare no competing financial interest.

■ ACKNOWLEDGMENTS

The synthesis, spectroscopic characterization, and modeling work performed at Rutgers, UT Dallas, and Wake Forest was supported in its totality by the Department of Energy, Basic Energy Sciences, division of Materials Sciences and Engineering (DOE Grant No. DE-FG02-08ER46491). The isotherm measurements, performed at PNNL, were supported by the U.S. Department of Energy, Office of Basic Energy Sciences, Division of Materials Sciences and Engineering (Award No. KC020105-FWP12152). Pacific Northwest National Laboratory is operated by Battelle for the U.S. Department of Energy under Contract No. DE-AC05-76RL01830.

■ REFERENCES

- Wu, H.; Gong, Q.; Olson, D. H.; Li, J. *Chem. Rev.* **2012**, *112*, 836.
- Zhou, H.-C.; Long, J. R.; Yaghi, O. M. *Chem. Rev.* **2012**, *112*, 673.
- Sumida, K.; Rogow, D. L.; Mason, J. A.; McDonald, T. M.; Bloch, E. D.; Herm, Z. R.; Bae, T.-H.; Long, J. R. *Chem. Rev.* **2011**, *112*, 724.
- Suh, M. P.; Park, H. J.; Prasad, T. K.; Lim, D.-W. *Chem. Rev.* **2011**, *112*, 782.
- Wu, H.; Zhou, W.; Yildirim, T. *J. Am. Chem. Soc.* **2009**, *131*, 4995.
- Li, B.; Zhang, Z.; Li, Y.; Yao, K.; Zhu, Y.; Deng, Z.; Yang, F.; Zhou, X.; Li, G.; Wu, H.; Nijem, N.; Chabal, Y. J.; Lai, Z.; Han, Y.; Shi, Z.; Feng, S.; Li, J. *Angew. Chem., Int. Ed.* **2012**, *51*, 1412.
- Li, K.; Olson, D. H.; Seidel, J.; Emge, T. J.; Gong, H.; Zeng, H.; Li, J. *J. Am. Chem. Soc.* **2009**, *131*, 10368.
- Pan, L.; H. Olson, D.; R. Ciemnomolonski, L.; Heddy, R.; Li, J. *Angew. Chem., Int. Ed.* **2006**, *45*, 616.
- Pan, L.; Parker, B.; Huang, X.; Olson, D. H.; Lee, J. *J. Am. Chem. Soc.* **2006**, *128*, 4180.
- Horcajada, P.; Gref, R.; Baati, T.; Allan, P. K.; Maurin, G.; Couvreur, P.; Férey, G.; Morris, R. E.; Serre, C. *Chem. Rev.* **2011**, *112*, 1232.
- Li, J.-R.; Sculley, J.; Zhou, H.-C. *Chem. Rev.* **2011**, *112*, 869.
- Fernandez, C. A.; Thallapally, P. K.; Motkuri, R. K.; Nune, S. K.; Sumrak, J. C.; Tian, J.; Liu, J. *Cryst. Growth Des.* **2010**, *10*, 1037.
- Thallapally, P. K.; Motkuri, R. K.; Fernandez, C. A.; McGrail, B. P.; Behrooz, G. S. *Inorg. Chem.* **2010**, *49*, 4909.
- López, D.; Buitrago, R.; Sepúlveda-Escribano, A.; Rodríguez-Reinoso, F.; Mondragón, F. *J. Phys. Chem. C.* **2008**, *112*, 15335.
- Lizzio, A. A.; DeBarr, J. A. *Fuel* **1996**, *75*, 1515.
- Lizzio, A. A.; DeBarr, J. A. *Energy Fuels* **1997**, *11*, 284.
- Srinivasan, A.; Grutzeck, M. W. *Environ. Sci. Technol.* **1999**, *33*, 1464.
- Shor, A. M.; Rubaylo, A. I. *J. Mol. Struct.* **1997**, *410–411*, 133.
- Marcu, I. C.; Sandulescu, I. *J. Serb. Chem. Soc.* **2004**, *69*, 563.
- Britt, D.; Tranchemontagne, D.; Yaghi, O. M. *Proc. Natl. Acad. Sci.* **2008**, *105*, 11623.
- Grant Glover, T.; Peterson, G. W.; Schindler, B. J.; Britt, D.; Yaghi, O. *Chem. Eng. Sci.* **2011**, *66*, 163.
- Liao, P.-Q.; Zhou, D.-D.; Zhu, A.-X.; Jiang, L.; Lin, R.-B.; Zhang, J.-P.; Chen, X.-M. *J. Am. Chem. Soc.* **2012**, *134*, 17380.
- Cui, P.; Ma, Y.-G.; Li, H.-H.; Zhao, B.; Li, J.-R.; Cheng, P.; Balbuena, P. B.; Zhou, H.-C. *J. Am. Chem. Soc.* **2012**, *134*, 18892.
- Yang, S.; Sun, J.; Ramirez-Cuesta, A. J.; Callear, S. K.; DavidWilliam, I. F.; Anderson, D. P.; Newby, R.; Blake, A. J.; Parker, J. E.; Tang, C. C.; Schröder, M. *Nat. Chem.* **2012**, *4*, 887.
- Thonhauser, T.; Cooper, V. R.; Li, S.; Puzder, A.; Hyldgaard, P.; Langreth, D. C. *Phys. Rev. B* **2007**, *76*, 125112.
- Langreth, D. C.; Lundqvist, B. I.; Chakarova-Kack, S. D.; Cooper, V. R.; Dion, M.; Hyldgaard, P.; Kelkkanen, A.; Kleis, J.; Kong, L.; Li, S.; Moses, P. G.; Murray, E.; Puzder, A.; Rydberg, H.; Schroder, E.; Thonhauser, T. *J. Phys.: Condens. Matter.* **2009**, *21*, 084203.
- Kresse, G.; Hafner, J. *Phys. Rev. B* **1993**, *47*, 558.
- Kresse, G.; Hafner, J. *Phys. Rev. B* **1994**, *49*, 14251.
- Kresse, G.; Furthmüller, J. *Comput. Mater. Sci.* **1996**, *6*, 15.
- Kresse, G.; Furthmüller, J. *Phys. Rev. B* **1996**, *54*, 11169.
- Yao, Y.; Nijem, N.; Li, J.; Chabal, Y. J.; Langreth, D. C.; Thonhauser, T. *Phys. Rev.* **2012**, *85*, 064302.
- Canepa, P.; Nijem, N.; Chabal, Y. J.; Thonhauser, T. *Phys. Rev. Lett.* **2013**, *110*, 026102.
- Nijem, N.; Canepa, P.; Kong, L.; Wu, H.; Li, J.; Thonhauser, T.; Chabal, Y. J. *J. Phys.: Condens. Matter* **2012**, *24*, 424203.
- Nijem, N.; Wu, H.; Canepa, P.; Marti, A.; Balkus, K. J.; Thonhauser, T.; Li, J.; Chabal, Y. J. *J. Am. Chem. Soc.* **2012**, *134*, 15201.
- Tan, K.; Nijem, N.; Canepa, P.; Gong, Q.; Li, J.; Thonhauser, T.; Chabal, Y. J. *Chem. Mater.* **2012**, *24*, 3153.
- Blöchl, P. E. *Phys. Rev. B.* **1994**, *50*, 17953.
- Kresse, G.; Joubert, D. *Phys. Rev. B.* **1999**, *59*, 1758.
- Kong, L. Z.; Cooper, V. R.; Nijem, N.; Li, K. H.; Li, J.; Chabal, Y. J.; Langreth, D. C. *Phys. Rev. B.* **2009**, *79*, 081407.
- Henkelman, G.; Arnaldsson, A.; Jónsson, H. *Comput. Mater. Sci.* **2006**, *36*, 354.
- Canepa, P.; Hanson, R. M.; Ugliengo, P.; Alfredsson, M. *J. Appl. Crystallogr.* **2011**, *44*, 225.
- Dybtssev, D. N.; Chun, H.; Kim, K. *Angew. Chem., Int. Ed.* **2004**, *43*, 5033.
- Maniam, P.; Stock, N. *Inorg. Chem.* **2011**, *50*, 5085.
- Lee, J. Y.; Olson, D. H.; Pan, L.; Emge, T. J.; Li, J. *Adv. Funct. Mater.* **2007**, *17*, 1255.
- Song, P.; Li, Y.; He, B.; Yang, J.; Zheng, J.; Li, X. *Microporous Mesoporous Mater.* **2011**, *142*, 208.
- Kizzie, A. C.; Wong-Foy, A. G.; Matzger, A. J. *Langmuir* **2011**, *27*, 6368.
- Liang, Z.; Marshall, M.; Chaffee, A. L. *Microporous Mesoporous Mater.* **2010**, *132*, 305.
- Arstad, B.; Fjellvåg, H.; Kongshaug, K.; Swang, O.; Blom, R. *Adsorption* **2008**, *14*, 755.
- Herzberg, G. *Molecular Spectra and Molecular Structure*; Krieger Pub Co.: Malabar, FL, 1950; Vol. 1.
- Goodman, A. L.; Li, P.; Usher, C. R.; Grassian, V. H. *J. Phys. Chem. A* **2001**, *105*, 6109.

- (50) Schneider, W. F.; Li, J.; Hass, K. C. *J. Phys. Chem. B* **2001**, *105*, 6972.
- (51) Chen, Y. F.; Lee, J. Y.; Babarao, R.; Li, J.; Jiang, J. W. *J. Phys. Chem. C* **2010**, *114*, 6602.
- (52) Rodriguez, J. A.; Jirsak, T.; Freitag, A.; Larese, J. Z.; Maiti, A. *J. Phys. Chem. B* **2000**, *104*, 7439.
- (53) Rodriguez, J. A.; Jirsak, T.; Chaturvedi, S.; Dvorak, J. J. *Mol. Catal. A: Chem.* **2001**, *167*, 47.
- (54) Chaturvedi, S.; Rodriguez, J. A.; Jirsak, T.; Hrbek, J. *J. Phys. Chem. B* **1998**, *102*, 7033.
- (55) Stark, J. V.; Klabunde, K. J. *Chem. Mater.* **1996**, *8*, 1913.
- (56) Nakamoto, K. *Infrared and Raman Spectra of Inorganic and Coordination Compounds*, 6th ed.; Wiley & Sons, Inc.: Hoboken, NJ, 2009.
- (57) Chen, B.; Ma, S.; Zapata, F.; Lobkovsky, E. B.; Yang, J. *Inorg. Chem.* **2006**, *45*, 5718.
- (58) Zhang, Z.; Liu, J.; Li, Z.; Li, J. *Dalton Trans.* **2012**, *41*, 4232.
- (59) Zheng, W.; Lau, K.-C.; Wong, N.-B.; Li, W.-K. *Chem. Phys. Lett.* **2009**, *467*, 402.
- (60) Taleb-Bendiab, A.; Hillig li, K. W.; Kuczkowski, R. L. *J. Chem. Phys.* **1992**, *97*, 2996.
- (61) Attila, Szabo; Ostlund, N. S. *Modern Quantum Chemistry: Introduction to Advanced Electronic Structure Theory*; Dover Publications, Inc.: Mineola, NY, 1996.
- (62) Shimanouchi, T. *J. Phys. Chem. Ref. Data* **1977**, *6*, 993.